

Article

A Comparative Study on the Crystalline and Surface Properties of Carbonized Mesoporous Coconut Shell Chars

Zaib Un Nisa ^{1,*} , Lee Kean Chuan ¹ , Beh Hoe Guan ¹, Faiz Ahmad ² and Saba Ayub ¹ 

¹ Department of Fundamental and Applied Sciences, Universiti Teknologi Petronas, Seri Iskandar 32610, Perak, Malaysia

² Department of Mechanical Engineering, Universiti Teknologi Petronas, Seri Iskandar 32610, Perak, Malaysia

* Correspondence: zaib_20001001@utp.edu.my

Abstract: In the present work, the facile thermal decomposition of raw coconut shells was carried out for the exploitation of the role of inert gas in the carbonization process and its role in determining the morphology, crystallographic parameters, and surface area of biochar before activation. The comparative investigation of mesoporous carbonized products synthesized with the muffle and tube furnace was carried out at a similar temperature and an assessment was made with a commercial carbon. The focus of the work was aimed at the interpretation of surface morphology, elemental identification, phase composition, interplanar spacing, full-width half maximum, crystallite size, lateral size, number of layers, dislocation density, microstrain, packing density, crystallinity index, and the specific surface area of the product obtained from two different approaches. It was revealed that the carbonized coconut shell chars obtained from the tube furnace have better characteristics to be activated further for carbon black synthesis. So, the flow of inert gas in a tube furnace is demonstrated to have a key role in improving the attributes of coconut shell chars.

Keywords: synthesis; thermal decomposition; carbonization; biochar; coconut shell chars; carbon black; mesoporous



Citation: Nisa, Z.U.; Chuan, L.K.; Guan, B.H.; Ahmad, F.; Ayub, S. A Comparative Study on the Crystalline and Surface Properties of Carbonized Mesoporous Coconut Shell Chars. *Sustainability* **2023**, *15*, 6464. <https://doi.org/10.3390/su15086464>

Academic Editors: Zheng Lu, Jiafei Jiang and Tengfei Fu

Received: 23 February 2023

Revised: 10 March 2023

Accepted: 14 March 2023

Published: 11 April 2023



Copyright: © 2023 by the authors. Licensee MDPI, Basel, Switzerland. This article is an open access article distributed under the terms and conditions of the Creative Commons Attribution (CC BY) license (<https://creativecommons.org/licenses/by/4.0/>).

1. Introduction

Carbon black is emerging as one of the most economical, as well as recurrently, used materials in various industries in modern applications. Owing to its porous structure, it can be effectively modified and, in the activated form, can be utilized for wastewater treatment and other adsorption purposes [1,2]. Effective practical utilization of carbon black has encouraged an increasing demand for the production of low-budget carbon black. Bio-carbon obtained from agricultural waste is a potent material to synthesize carbon black because of its cost-effective advantages and low levels of inorganic compounds. Carbon black is known as one of the copiously formed materials of carbon, and it is estimated that roughly seventy percent of it is utilized as a pigment, as filler/reinforcement in rubber, and as elastomeric materials. The utilization of rubber in different applications relying on the addition of carbon black has been investigated for more than a hundred years [3].

Renewable energy sources and carbon capture applications are the current scientific verdict statements on other usages of carbon black that are of considerable attention [4]. Other key areas for the consumption of black carbon are now applicable to modern worldwide challenges, highlighting especially cleaner production, energy, various sensors [5,6], dielectric and electromagnetic interference materials [7], high-performance batteries [8], and polymer modifications [9]. Current exploration has also extended the chemistry of carbon black to utilize it as a starting material for quantum dots of graphene and hollow spheres of carbon for extending its employment in the renewable energy sector in storage devices for electrochemical energy and remedy of the environment [10]. Subsequently, the carbon black nanostructural product in the current methodologies is utilized for the grafting of polymers because functional groups are translated to carbon black with ease [11].

Different carbon-containing natural materials (such as plant wood, agricultural waste, hardened shells of nuts, peat, lignite, char, coal) and amorphous porous materials (such as biochar, carbon gels, etc.) are utilized as common sources of raw material to produce activated carbon [12–17]. The crop's routine need of the creatures on earth and their production led to excessive by-products and residual waste on the planet. These agricultural wastes are inexpensive and their fruitful consumption can be made by transforming these into useful products [18]. As a result, the high surface area containing carbon products can be synthesized easily using agricultural by-products [19]. Most of the biowastes are now utilized for the production of commercial carbon products. The abundance in availability of inexpensive agricultural raw materials and by-products supports their utilization [20].

Carbon black prepared from agricultural waste is used as an electrode material and supercapacitors in electronic devices [21–25]. Due to the inherently high surface area, in-built porosity, and easy tailoring ability, the synthesized material can meet the requirement of devices used for energy storage [26,27]. Carbon black can be used to increase electrical conductance. Composites of insulated polymers can be fabricated using conductive fillers, including carbon black [28]. It can be easily dispersed in an insulating matrix to get a composite with increased conductivity [29]. Polymer composites prepared using carbon-based materials are useful candidates for shielding applications [30]. The characteristics of the carbon black can also be varied depending on carbonization conditions, so optimization of carbonization conditions can be achieved by the appropriate selection of the heating rate and the activation temperature [31]. It has been reported that the physical and chemical characteristics of carbon depend upon the source of origin or raw material used [32]. One of the characteristics that distinguish a product from one another is the material composition (i.e., hemicellulose, cellulose, or lignin) [33]. Carbon black showed microstructural variations depending on heat treatment. This knowledge is helpful to understand the role of heat-treatment practices such as carbonization, physical activation, chemical activation, graphitization, and stabilizing the product.

It is a known fact that carbon-based materials (such as carbon black, chars, or activated carbon) have demonstrated fine pore-size development than wood-based carbon products. The majority of the pores have shown a radius in nanometers, in the case of coconut shells, while carbon material originating from other woods has a significant number of macropores and mesopores [34,35]. Black nanocarbon, specifically obtained from coconut shells as a bio-carbon source, has the potential for substituting the conventional thermoset filler in wear applications due to their high strength, low density, hardness, abrasion resistance, and modulus properties [36,37]. It is reported that to produce mesoporous or macroporous material, lignocellulosic material is useful [38]. Herein coconut shell also contains lignin as the major ingredient (i.e., 29.35%) so most of the pores are macro or mesoporous [39]. The mesoporous-carbon coconut shell is a suitable raw material because it carries superb natural structure and possesses relatively a smaller ash as a by-product [40]. By exposing the coconut shell to different experimental conditions, the structure and porosity of the activated carbon can be assessed.

The main focus of the current study is to provide a possibly inexpensive and low-cost carbonized product from agricultural wastes as a substitute for the synthesis of the current commercial carbon black [41,42]. Carbon black is manufactured globally in tons each year because of its reasonably low associated cost compared to other conductive substances. Commercially, carbon is used in several industrial progressions and operations, such as the gasification of coal, ethanol synthesis, manufacture of fertilizer, natural gas production, refinery processing, and composites synthesis [43–45]. Various activation techniques are available, however, the methods following non-activation techniques are useful for reducing the cost of manufactured materials [21].

Carbon materials, specifically mesoporous carbon, is an encouraging material having several applications. One of the crucial uses presented in the literature is through oral drug delivery systems [46–48], water purification [49–51], adsorbing media for the substrates [52,53], and catalytic support [54,55]. There has been literature available us-

ing thermal, XRD (X-ray Powder Diffraction), and BET (Brunauer, Emmet, and Teller) analysis of biochar of plant waste [56,57]. Comparative studies are available for different carbonization and activation methods [58–60], but no information is available about the char's characteristics before activation. Gas flow can affect the surface properties of the material, so samples prepared in a tube furnace can have altered properties when compared with a muffle furnace. Activation of material through physical means is known as one of the easiest ways to increase the adsorption capacity of a surface [61,62]. There is an observed lack of literature in a comparative investigation of the role of inert gas in determining the surface area of carbonized products. The basic difference between a tube and a muffle furnace is the circulation of inert gas. The inert gas is missing in a muffle furnace, so considering it the easiest way for a comparative study of the role of the inert gas current research was conducted using the carbonization method. The focus is given to investigating the properties of the mesoporous carbonized product synthesized using two extremely facile fundamental thermal decomposition processes. The purpose of the study is to explore the surface morphology, estimation of elemental composition, XRD parameters, and surface characteristics of carbonized products developed by facile thermal decomposition strategy. The comparison of properties is also made with product available activated commercial carbon black (CP).

2. Experimental

2.1. Raw Materials

Coconut shells were used as raw materials to produce mesoporous carbon. The coconut shells were cleaned with distilled water. The drying of the cleaned coconut shell was carried out in an oven at 80 °C. The granulation of coconut was carried out in a granulator (SHINI, China Model No. SG-21P) to get smaller-sized naked particles. Carbon nanopowder (CP) with stock no US1078 size (<100 nm) was purchased from the US Research Nanomaterials, Inc. (Houston, TX, USA) for a comparative study.

2.2. Thermal Decomposition of Coconut Shells

The granules of coconut shells were thermally degraded in the following way.

a. Muffle Furnace sample (MFCB)

The ceramic boat was loaded with granules of coconut shells and mounted in a muffle furnace (PROTHERM, France Model: PLF 120/15) with dimensions $D \times W \times H = 30 \times 22 \times 23$ cm at 400 °C for 2 h. After giving the annealing time of 6 h, the product was removed and ground in a laboratory blender (WARING, USA Model No. HGBTWTG4) to get powder. The powder product was sieved further to get the mesoporous product. The powder was further sieved using 3 U.S. mesh to get the product (Figure 1).

b. Tube Furnace sample (TFCB)

The ceramic boat was filled with granules of coconut shells and heated inside a tube furnace (PROTHERM, France model: PTF 12/75/800, dimensions: $D \times W \times H = 635 \times 850 \times 400$, tube type: C610) at a temperature of 400 °C at a heating rate of 5 °C/min for 2 h under an inert atmosphere of N₂. After carbonization, the product was cooled to room temperature and after annealing for 6 h, it was ground in a laboratory blender to get powder. The carbonized product was obtained by sieving the product. The carbonized product given in Figure 1 was obtained by sieving the product with 3 U.S. mesh.

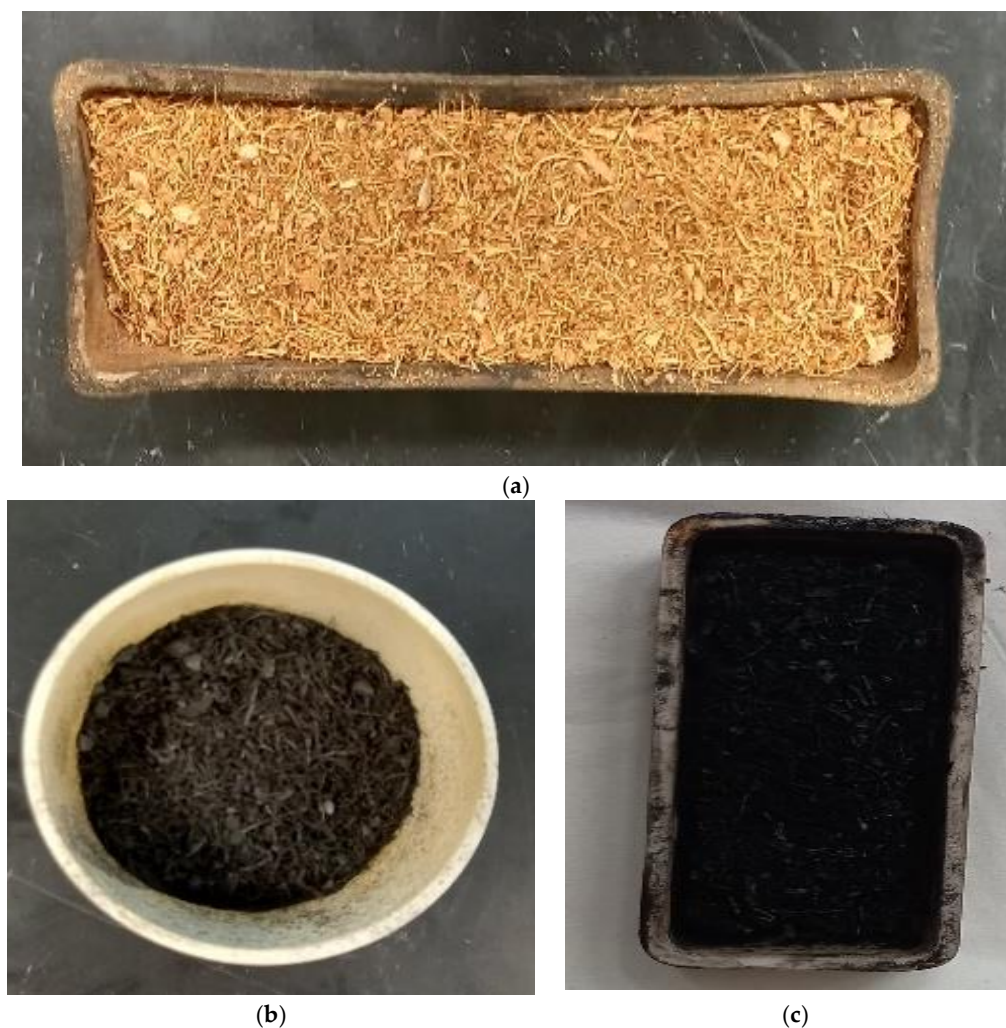


Figure 1. Samples of coconut shell (a) Before treatment, (b) After treatment in a muffle furnace (c) After treatment in the tube furnace.

2.3. Characterization

Three characterization techniques were utilized to study morphology, elemental identification, phase composition, crystallinity, particle size, dimension, and specific surface area of the carbonized product. The field-emission scanning electron microscope (FESEM) imaging, along with the elemental distribution spectra (EDS), was obtained using Carl Zeiss, Germany (Supra 55vp) instrument.

An X-ray Powder Diffraction (XRD) analysis was carried out on (Bruker, Germany AXS, D8 advance) instrument with $\text{Cu K}\alpha$ ($\lambda_1 = 1.54056 \text{ \AA}$ & $\lambda_2 = 1.5444 \text{ \AA}$ with a ratio of $\lambda_2/\lambda_1 = 0.5$) radiation source (45 kV & 40 mA) in continuous scanning mode. The samples were analyzed at a scanning speed of 1° min^{-1} from 10° to 100° on a 2θ scale.

The surface area and particle size (SAP) analysis was performed on Micromeritics, USA (ASAP 2020) instrument to measure the specific surface area of the material. Brunauer-Emmett-Teller's theory aims to explain the physical adsorption of gas molecules on a solid surface and serves as the basis for an important analysis technique for the measurement of the specific surface area of materials.

3. Results and Discussion

The carbonized products in the TFCB and the MFCB were prepared at the same carbonization temperature of 400°C . The TFCB was supplied with a constant flow of nitrogen gas at $5^\circ \text{C}/\text{min}$. Both products were characterized and compared with the commercial product using the following techniques.

3.1. Surface Morphology and Composition

The MFCB and the TFCB mesoporous products were prepared using the thermal decomposition method. FESEM imaging, with the EDS, is a useful microscopic analytical technique. The surface characterization of the carbonized material, in terms of morphology and composition, was achieved using this technique. The images presented in Figure 2 were captured at an acceleration potential of 5 to 15 kV using different magnifications. The mesopores are pores classified in the nanoscale range (from 2 to 50 nm), thus, these pores are not visible in the presented scale range. The visible pores present in the FESEM images of the TFCB and the MFCB are macropores (pores larger than 50 nm) [63]. Such pores are not manifested in the CP at a given magnification. As a result, the CP shows different morphological behavior at observed analytical conditions.

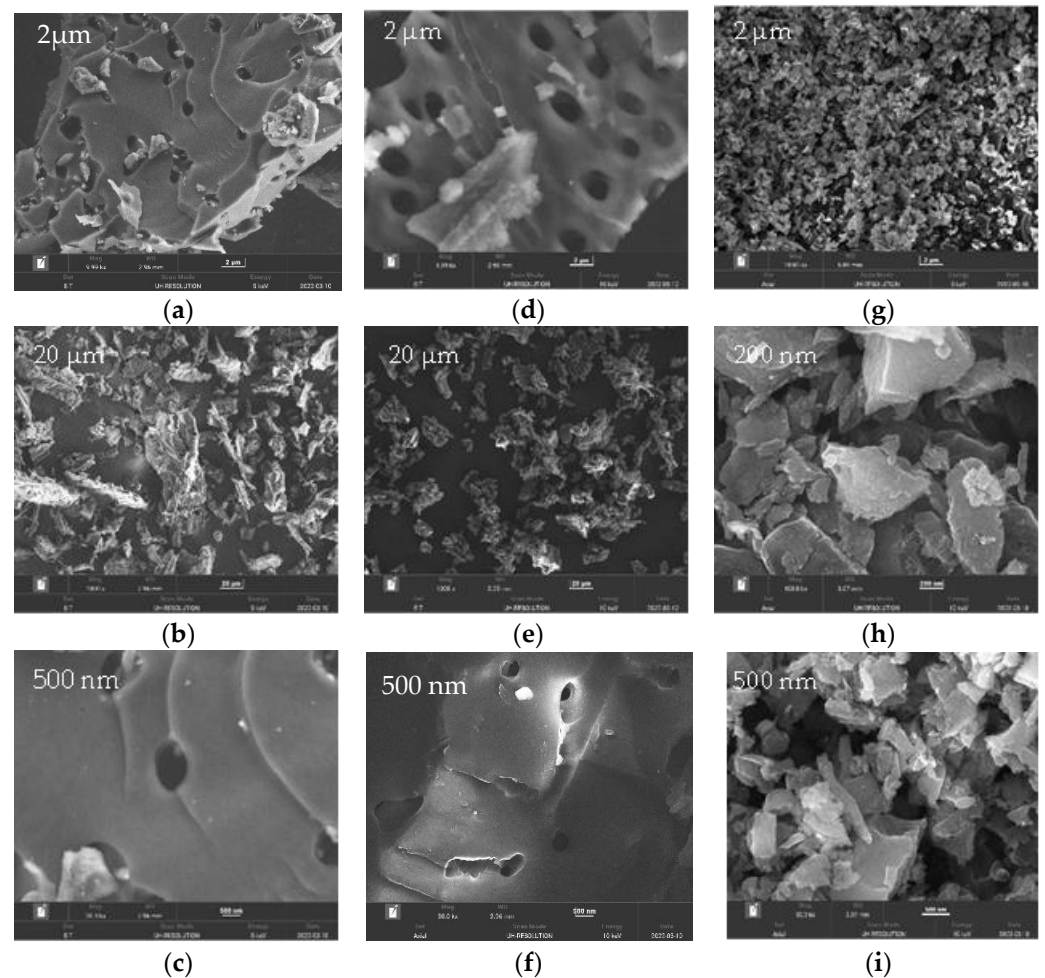


Figure 2. FESEM images of carbonized products (a) TFCB at 2 μm , (b) TFCB at 20 μm , (c) TFCB at 500 nm, (d) MFCB at 2 μm , (e) MFCB at 20 μm , (f) MFCB at 500 nm, (g) CP at 2 μm , (h) CP at 200 nm, and (i) CP at 500 nm.

Backscattered electron (BSE) and the elemental distribution spectra (EDS) are presented in Figures 3 and 4, respectively. This explains the complementary evidence of the chemistry of the subsurface and the morphology of the product. The EDS depicts that obtaining the mesoporous product from a tube furnace, having a flow of nitrogen inert gas, has resulted in 78.3% carbon in the end product with some residual amounts of sodium, potassium, and chlorine from the coconut shell ingredients. However, the product obtained from the muffle furnace possesses a smaller content of mesoporous carbon (i.e., 75.2% only). According to the results, both products showed some common residual contents in the form of potassium, chlorine, and sodium. The product MFCB is owing some additional inorganic ingredients in the form of magnesium, phosphorous, and sulfur.

The carbonization technique breaks down the intricate carbonaceous material using air for the burning purpose and the complex ingredients of the source are degraded into carbon and other elemental precursors [64]. It is assumed from the finding that the spontaneous degradation or breakdown of the same source material during different carbonization atmospheres gives different residual elements in the end product. A muffle furnace is using atmospheric conditions for the oxidation of coconut shells, while a tube furnace is using inert atmosphere. The oxygen percentage of the product observed in the muffle furnace is more compared with the tube furnace showing a greater possibility of the formation of oxidized products. In a tube furnace, due to controlled inert conditions, the pyrolysis is maximum, and the breakdown of the product happens with a greater loss of ingredients and less yield of oxidized products in the char.

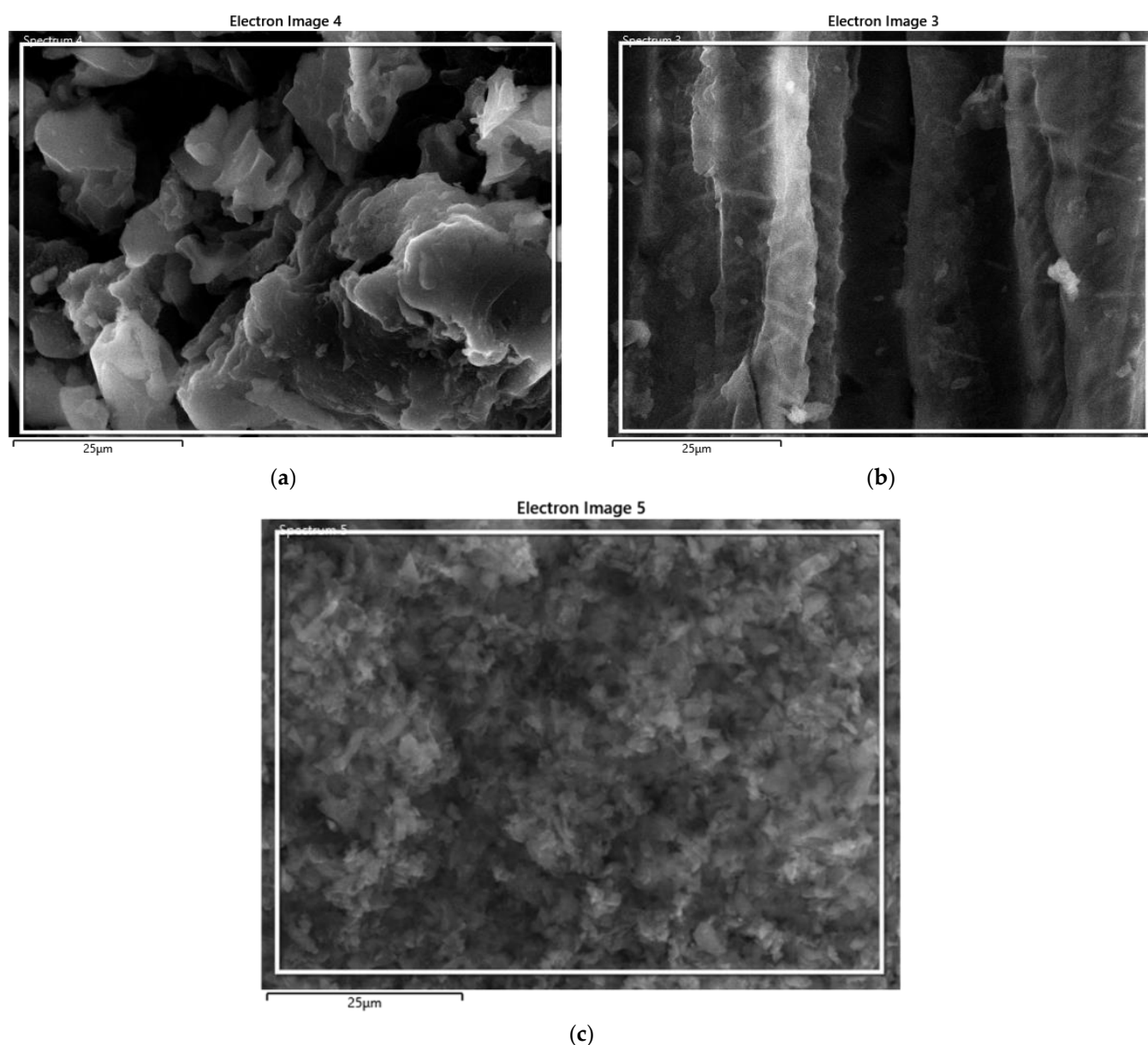
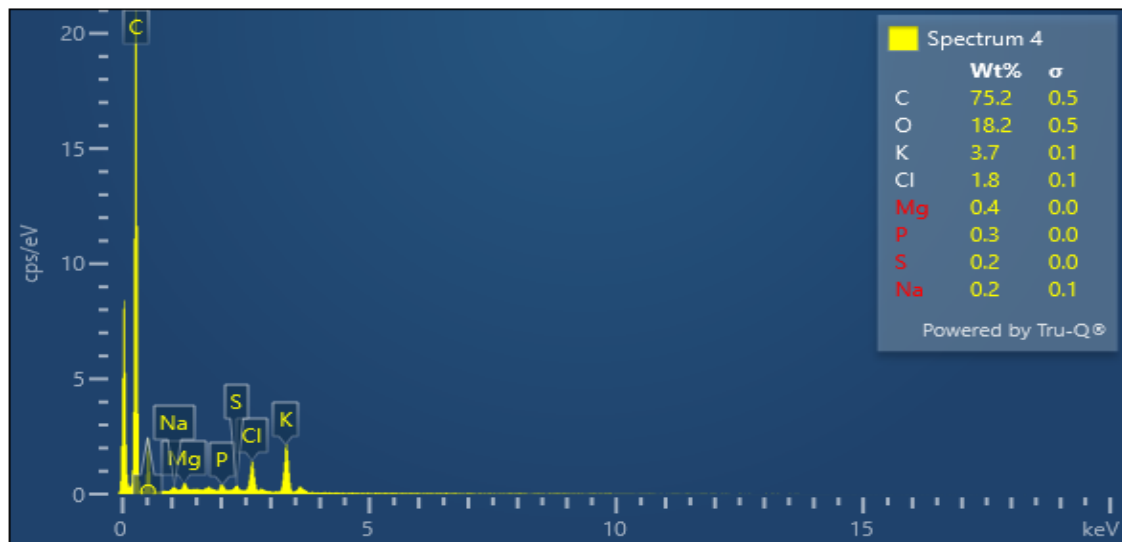
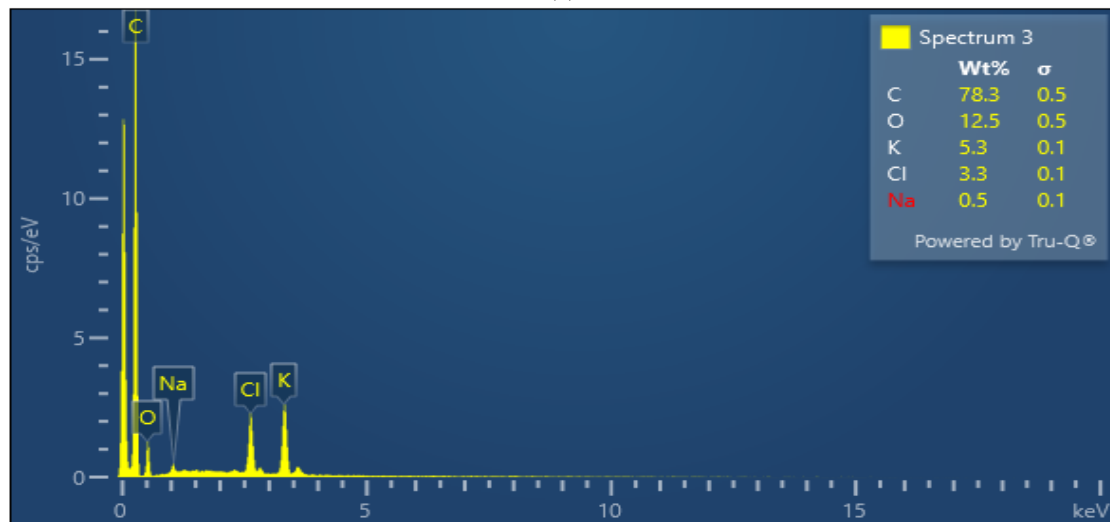


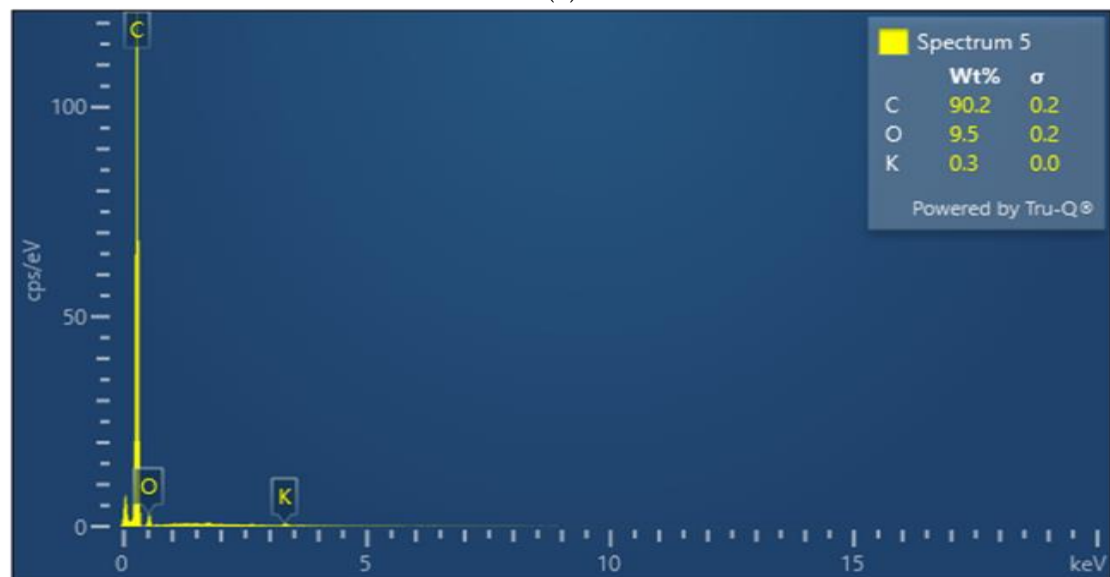
Figure 3. BSE images of carbonized products (a) BSE image of MFCB, (b) BSE image of TFCB, and (c) BSE image of CP.



(a)



(b)



(c)

Figure 4. EDS spectra of the carbonized products (a) EDS spectra of MFCB, (b) EDS spectra of TFCB, and (c) EDS spectra of CP.

The morphology of the MFCB and the TFCB products is also compared with the available commercial product, CP. Macropores are not observed in the CP at the given magnification. However, the EDS spectra of the CP are found to have 90.2% carbon content, which indicated fewer residual constituents are present in the starting material. Most of the inorganic constituents are found to be missing in the CP. Less carbon content in the TFCB and the MFCB is assumed to be present due to residual contents of coconut shells which are absent in the purchased commercial product. The source of the commercial product was not known. It is assumed that the variation in the percentage of carbon and inorganic content in the EDS spectra of the CP is due to the difference in the composition of raw materials and the synthesis procedure utilized.

3.2. X-ray Diffraction Analysis

The XRD pattern obtained for the mesoporous MFCB, TFCB, and CP is presented in Figure 5. Carbon black is a combination of heterogeneous particles whose thickness varies from mono graphitic layer to a multilayer arrangement. It shows a pattern consisting of two to three diffused rings. The position of spectral peaks in powder diffraction analysis is approximately at the same location as in the spectra of graphite. Sometimes it is assumed that carbon black is a fine-grained form of graphite with crystalline nature. However, studies have also demonstrated loose packing of grains with very little size, just like amorphous solids [65]. Therefore, it's not probable to predict the ratio of graphitic crystals and mesomorphic forms of carbon. Usually, the sloppy packing of particularly small particles gives rise to intense scattering at a small-scale angle. The analysis usually shows two clear Bragg peaks related to reflections from (002) and (10) planes.

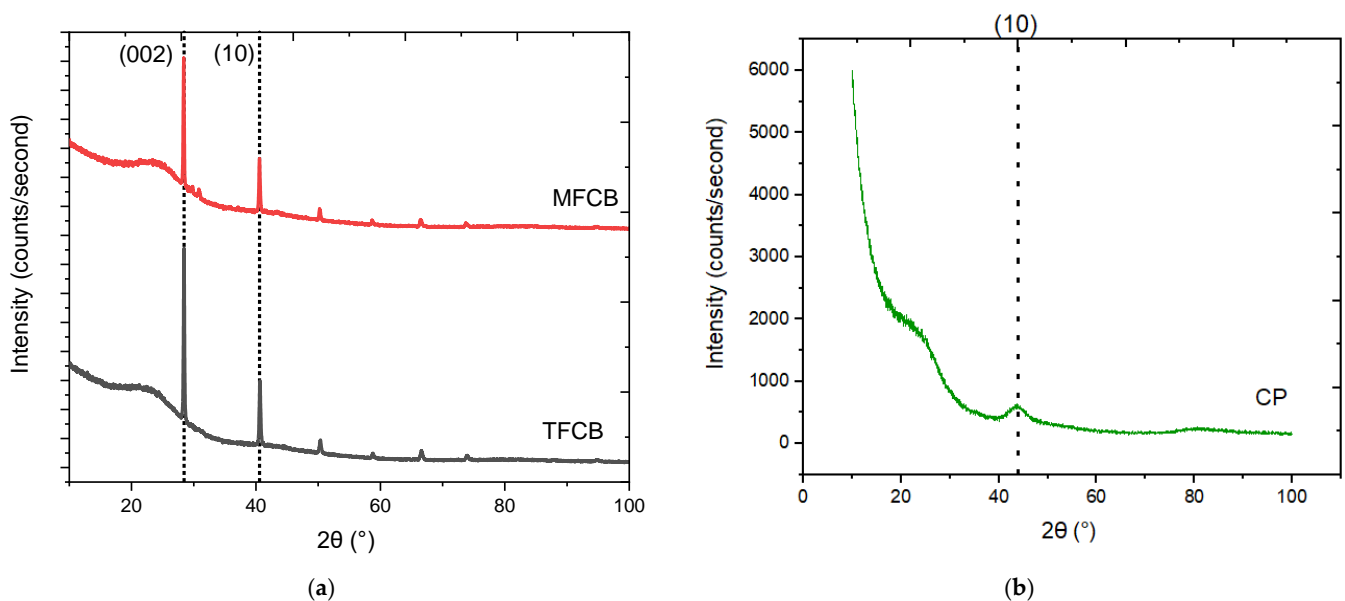


Figure 5. XRD spectral pattern of (a) MFCB and TFCB, (b) CP.

The MFCB peak, due to the reflection from the (002) plane, is found to be major and intense at 28.3° on the 2θ scale. The second peak of two-dimensional reflection from the (10) plane is due to a graphite-like structure and is present at 40.5° on a 2θ scale. The TFCB also shows a similar pattern with the main reflection at 28.2° on the 2θ scale and due to two-dimensional reflection from the (10) plane at 40.4° on the 2θ scale. However, in the CP, only one peak is observed due to the graphitic structure at 40.3° and the peak due to (002) plane is not clear. Therefore, the commercial product has a pronounced peak at a larger angle with the indication of more amorphous characters. Further structural information, in terms of interplanar spacing (d_{hkl}), full-width half maximum (FWHM), the crystallite size (L_c), lateral size (L_a), the number of layers (N), dislocation density (δ), microstrain (ϵ), packing density (ρ), and crystallinity index (I), were determined using the

formula from the literature [36] and presented in Table 1 for the MFCB and the TFCB. There exist controversies among the results of the microstructural calculations as the results are unpredictable. The reason behind such variations is unknown. One of the major factors is found to be the oxidation method or heat-treatment procedure [66]. Small changes in the operating conditions can give the product different characteristics [67].

Table 1. Structural information of samples determined from XRD patterns.

Parameter	MFCB	TFCB	CP
d_{002} (Å)	3.15	3.16	-
d_{10} (Å)	2.22	2.22	2.23
FWHM	0.21	0.22	7.2
L_c (nm)	37.93	36.63	1.17
L_a (nm)	81.77	78.97	2.53
N (Items)	12.03	12.79	0.53
δ (nm ⁻²)	0.69	0.74	723
ϵ ($\times 10^{-3}$)	3.73	3.88	85.6
ρ (g/cm ³)	0.24	0.26	0.34
Crystallinity Index (%)	25.8	23.4	13

The microstructural parameters show that the interplanar spacing of all three samples is almost the same. The crystalline size and lateral size of the TFCB are better than the MFCB. The number of layers in each stack and packing density is found to be greater for the TFCB than for the MFCB. There is an observed difference of 0.02 g/cm³ in packing density between the MFCB and the TFCB, which highlighted the fact that the TFCB sample is more compact and ordered compared with the MFCB.

The smaller the crystalline size, the lower the degree of graphitization will be [36]. The CP is observed to have the greatest interplanar spacing with the greatest FWHM, as the peak is broader with small intensity. It is also observed that most of the calculated microstructural parameters of the CP are not comparable to the MFCB and the TFCB. The reason behind the observed variation is assumed to be the greater graphitic character. The dislocation density is found to be the highest for the CP, which also supports the greater amorphous properties in the commercial product. Similarly, N is calculated to be 12.03 and 12.79 for the MFCB and the TFCB respectively while it is negligible for the CP. As predicted, all the microscopic parameters calculated from the XRD data suggest that the size of the primary atoms in the TFCB is the smallest in the analyzed samples, which emphasizes the carbonization conditions to be favorable in the tube furnace. The X-ray Diffraction analysis was also used to predict the degree of crystallinity using the diffraction intensity ratio of the crystalline peak with the amorphous peak as it related to the respective mass ratios [68].

In the present work, the relative proportions of the amorphous and the crystalline were determined based on the maximum reflection peak from the (002) planes. The crystallinity index is calculated using Equation (1).

$$\text{Crystallinity Index (\%)} = (I_{\text{crystalline}}/I_{\text{total}}) \times 100 \quad (1)$$

The MFCB showed a crystallinity index of 25.8 %, compared to 23.4 % in the case of the TFCB. There is found to be a calculated difference of 2.4 %, which is attributed to the difference in processing conditions. Thus, nitrogen has displayed a critical role in the production of coconut shell chars with better properties. As per the prediction of determined microstructural parameters, the crystallinity calculation also presented a similar trend. The CP contains the least crystalline nature with 13% crystalline properties and a more graphitic character.

3.3. SAP Analysis

A solid adsorbent surface has been identified by the International Union of Pure and Applied Chemistry (IUPAC) to give five traditional types of isotherms [69]. The surface

area available for adsorption is associated with the size, volume, and diameter of the pores that are presented on a surface. This information was utilized to study the surface properties of the coconut shell chars. Following the classification given by the IUPAC, pores on adsorbent surfaces are categorized into three divisions:

- Micropores; pore size less than 2 nm;
- Mesopores; pore size ranging from 2–50 nm;
- Macropores; pore size greater than 50 nm.

Properties related to the surface of a material can be predicted by studying the physical adsorption phenomena. Brunauer-Emmett-Teller's theory aims to explain the physical adsorption of gas molecules on a solid surface and serves as the basis for an important analysis technique for the measurement of the specific surface area of materials. The driving force behind the physical adsorption of a substance is believed to be London dispersion forces. In some cases, electrostatic forces also play an important role in trapping adsorbate on the surface under observation.

The obtained isotherm linear plot at the STP for the MFCB and the TFCB samples is presented in Figure 6. The SAP analysis showed smooth type III isotherm, predicting stronger adsorbent adsorbate interactions according to the IUPAC classification. In the isotherm, the adsorption and desorption curves are abbreviated as Ad and De respectively. The initial region of the linear isotherm plot of the isotherm for all samples represents the saturation of the micropore with the nitrogen gas filling indicated by a rise in the adsorbed quantity of adsorbate. This is followed by a regular decrease in adsorbed gas with a rise in temperature in the form of desorption.

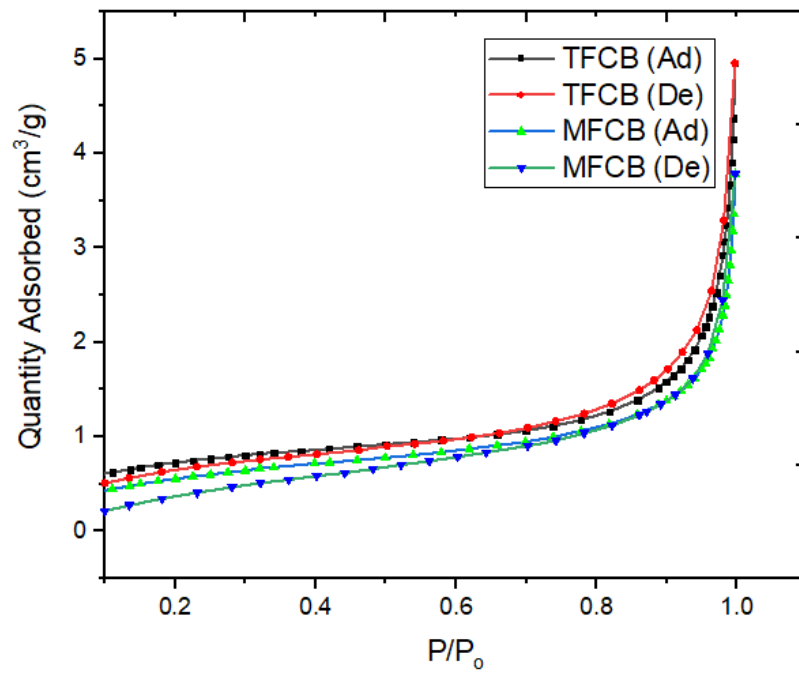
It was revealed that the size, diameter, and volume of pores that are present on a material have an important role in porosity developed specific surface area obtainable for effective adsorption, which, ultimately, determines the number and size of particles that can be easily diffused into the adsorbent. All of these are directly related to processing conditions which are the same for the synthesized samples except for the nitrogen gas, thus, it has a leading role in the determination of properties. As a suitable structure with the required pore parameters is of major concern for adsorption applications [70], processing conditions must be regulated because the activation process plays a major role in pore growth and improvement [71,72].

The surface was investigated for the change in relative pressure of nitrogen gas from 0.1 to 1, at $P/P_0 = 1.029$. All the active sites are exposed to adsorbate gas molecules having the same kinetics energy, so the adsorbate interactions are independent of the neighboring active sites. The absorption of the adsorbate is related to the number of active sites available. The nature of the synthesized carbon shell char in all samples is mesoporous as the pore diameter lies above 2 nm in all samples. The results are listed in Table 2. The specific surface is found to be highest for samples synthesized under the flow of nitrogen gas as compared to the MFCB.

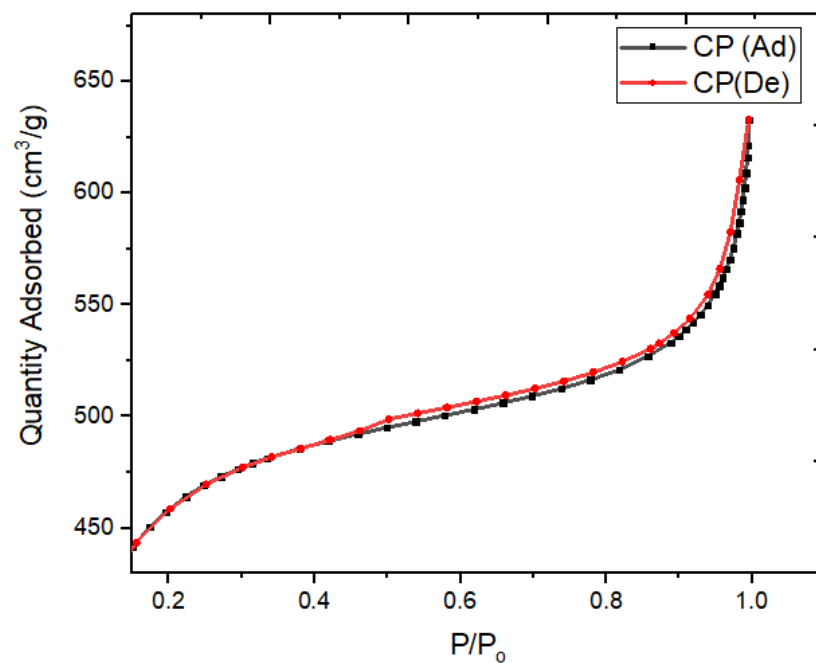
Therefore, the flow of nitrogen gas seems to have a prominent role in the physical modification of char, which, in turn, has resulted in a smaller pore diameter. While comparing the results of synthesized samples with those of commercial products, it can be noticed that it contains a higher surface area than the synthesized materials. As the commercial product was available in activated form, the additional activation step involved in a commercial sample raised the surface area of the product. The TFCB and the MFCB can be explored further following the activation step. It was revealed in the literature that the amorphous character can lead to a rise in the surface area of the product [72]. Although the commercial product has less crystalline character shown by the XRD, as it was in an activated form. Therefore, it has been more active toward absorption as shown by the SAP results. It was concluded that the surface properties of a material are independent of its crystalline or amorphous nature.

Table 2. SAP parameters of samples.

Sample	Specific Surface Area (S_{BET})	Langmuir Surface Area (S_L)	Average Pore Diameter (D)
MFCB	2.0827 m ² /g	3.3269 m ² /g	10.0844 nm
TFCB	2.5486 m ² /g	3.9141 m ² /g	9.4434 nm
CP	1517 m ² /g	2175 m ² /g	2.51232 nm



(a)



(b)

Figure 6. Isotherm Linear Plots of (a) MFCB, TFCB (b) CP.

4. Conclusions

The suitable pore characteristics, the number of pores developed on a solid surface during the synthesis protocol, and the achievement of an appropriate material for the carbon black synthesis are dependent upon the processing conditions and nature of the raw materials used. The commercial product was investigated to have an idea about the difference in surface morphology, crystallinity, XRD, and SAP parameters. The FESEM image reveals that on the surface of the product, clear macropores are also present, which were not observed in the commercial product. The carbon content is observed more in the commercial product compared with the TFCB and the MFCB, indicating the fact that coconut shell is also containing inorganic constituents. The XRD result revealed the introduction of incorporating more crystalline properties into the product synthesized using nitrogen flow. Only one peak is observed in the CP with less crystallinity and an indication of a graphitic peak only in the XRD analysis shows the improvement in lattice parameters and crystallinity of the TFCB as compared to the MFCB and the CP. The SAP analysis demonstrated that the nature of synthesized coconut shell char is mesoporous. Average pore diameter, specific surface area, and Langmuir surface area are found to be greater for the product of the tube furnace matched with the MFCB, which highlights the contribution of nitrogen gas in promoting the surface area. The work revealed the fact that by identifying the composition of the raw material carbon, and having a definite pore size, distribution can be produced. The ingredients of the CP are undisclosed as it was a commercial product. It can be assumed that its source of origin is containing less amount of lignin. It was revealed that the nitrogen gas circulation in the tube furnace has a role in the mesopore development and modification of char, in terms of its surface area. As a result, the soaking time of the process and activation of the product can be regulated further to explore the surface and crystalline properties of the synthesized chars. This study can be utilized for the production of mesoporous biochar which can be activated further by several reported methods. Activated carbon has found its immense use in several applications, such as industrial reinforcements, water purification, printing, high-performance coatings, polymer modification, and surface protection.

Author Contributions: Conceptualization, F.A.; Methodology, Z.U.N.; Formal analysis, S.A.; Investigation, B.H.G.; Writing—review & editing, Z.U.N.; Supervision, L.K.C. All authors have read and agreed to the published version of the manuscript.

Funding: This research received funding from centre of graduate studies UTP and Yayasan Universiti Teknologi Petronas (YUTP) cost centre 015CL0-333.

Institutional Review Board Statement: Not applicable.

Informed Consent Statement: Not applicable.

Data Availability Statement: Not applicable.

Acknowledgments: Department of Fundamental and Applied Sciences, Universiti Teknologi Petronas (UTP) is greatly acknowledged for this research.

Conflicts of Interest: The authors declare no conflict of interest.

Abbreviations

CP	Carbon nanopowder
XRD	X-ray Powder Diffraction
MFCB	Muffle furnace sample
FESEM	Field-emission scanning electron microscope
SAP	Surface area and particle size
De	Desorption
BET	Brunauer, Emmet, and Teller
TFCB	Tube furnace sample

BSE	Back scattered-electron
IUPAC	International union of pure and applied chemistry
STP	Standard temperature pressure
Ad	Adsorption

References

- Donyanavard, P. Production of Activated Carbon from Agricultural Waste and Investigation of Its Efficiency for Textile Wastewater Treatment. Master's Thesis, University of Manitoba, Winnipeg, MB, Canada, 2022.
- Sakhiya, A.K.; Anand, A.; Kaushal, P. Production, activation, and applications of biochar in recent times. *Biochar* **2020**, *2*, 253–285. [[CrossRef](#)]
- Robertson, C.G.; Hardman, N.J. Nature of Carbon Black Reinforcement of Rubber: Perspective on the Original Polymer Nanocomposite. *Polymers* **2021**, *13*, 538. [[CrossRef](#)] [[PubMed](#)]
- Khodabakhshi, S.; Fulvio, P.F.; Andreoli, E. Carbon black reborn: Structure and chemistry for renewable energy harnessing. *Carbon* **2020**, *162*, 604–649. [[CrossRef](#)]
- Ma, H.; Li, J.; Zhou, J.; Luo, Q.; Wu, W.; Mao, Z.; Ma, W. Screen-Printed Carbon Black/Recycled Sericin@Fabrics for Wearable Sensors to Monitor Sweat Loss. *ACS Appl. Mater. Interfaces* **2022**, *14*, 11813–11819. [[CrossRef](#)] [[PubMed](#)]
- Pagliero, M.; Alloisio, M.; Costa, C.; Firpo, R.; Mideksa, E.A.; Comite, A. Carbon Black/Polyvinylidene Fluoride Nanocomposite Membranes for Direct Solar Distillation. *Energies* **2022**, *15*, 740. [[CrossRef](#)]
- Liu, H.; Wu, S.; You, C.; Tian, N.; Li, Y.; Chopra, N. Recent progress in morphological engineering of carbon materials for electromagnetic interference shielding. *Carbon* **2021**, *172*, 569–596. [[CrossRef](#)]
- Xia, G.; Ye, J.; Zheng, Z.; Li, X.; Chen, C.; Hu, C. Catalytic FeP decorated carbon black as a multifunctional conducting additive for high-performance lithium-sulfur batteries. *Carbon* **2021**, *172*, 96–105. [[CrossRef](#)]
- Roy, N.; Sengupta, R.; Bhowmick, A.K. Modifications of carbon for polymer composites and nanocomposites. *Prog. Polym. Sci.* **2012**, *37*, 781–819. [[CrossRef](#)]
- Nguyen, V.-H.; Pazhouhanfar, Y.; Delbari, S.A.; Shaddel, S.; Babapoor, A.; Mohammadpourderakhshi, Y.; Van Le, Q.; Shokouhimehr, M.; Asl, M.S.; Namini, A.S. Beneficial role of carbon black on the properties of TiC ceramics. *Ceram. Int.* **2020**, *46*, 23544–23555. [[CrossRef](#)]
- Fan, Y.; Fowler, G.D.; Zhao, M. The past, present and future of carbon black as a rubber reinforcing filler—A review. *J. Clean. Prod.* **2020**, *247*, 119115. [[CrossRef](#)]
- Priya, D.S.; Kennedy, L.J.; Anand, G.T. Emerging trends in biomass-derived porous carbon materials for energy storage application: A critical review. *Mater. Today Sustain.* **2023**, *21*, 100320. [[CrossRef](#)]
- da Silva, E.L.; Torres, M.; Portugau, P.; Cuña, A. High surface activated carbon obtained from Uruguayan rice husk wastes for supercapacitor electrode applications: Correlation between physicochemical and electrochemical properties. *J. Energy Storage* **2021**, *44*, 103494. [[CrossRef](#)]
- Amaral-Labat, G.; Munhoz, M.G.C.; Fonseca, B.C.D.S.; Boss, A.F.N.; de Almeida-Mattos, P.; Braghiroli, F.L.; Bouafif, H.; Koubaa, A.; e Silva, G.F.B.L.; Baldan, M.R. Xerogel-like Materials from Sustainable Sources: Properties and Electrochemical Performances. *Energies* **2021**, *14*, 7977. [[CrossRef](#)]
- Braghiroli, F.L.; Passarini, L. Valorization of Biomass Residues from Forest Operations and Wood Manufacturing Presents a Wide Range of Sustainable and Innovative Possibilities. *Curr. For. Rep.* **2020**, *6*, 172–183. [[CrossRef](#)]
- Braghiroli, F.L.; Amaral-Labat, G.; Boss, A.F.N.; Lacoste, C.; Pizzi, A. Tannin Gels and Their Carbon Derivatives: A Review. *Biomolecules* **2019**, *9*, 587. [[CrossRef](#)]
- Amaral-Labat, G.; da Silva, E.L.; Cuña, A.; Malfatti, C.F.; Marcuzzo, J.S.; Baldan, M.R.; Celzard, A.; Fierro, V.; e Silva, G.F.B.L. A Sustainable Carbon Material from Kraft Black Liquor as Nickel-Based Electrocatalyst Support for Ethanol Electro-Oxidation. *Waste Biomass-Valorization* **2021**, *12*, 2507–2519. [[CrossRef](#)]
- Koul, B.; Yakoob, M.; Shah, M.P. Agricultural waste management strategies for environmental sustainability. *Environ. Res.* **2022**, *206*, 112285. [[CrossRef](#)]
- Zanzi, R.; Sjöström, K.; Björnbom, E. Rapid pyrolysis of agricultural residues at high temperature. *Biomass-Bioenergy* **2002**, *23*, 357–366. [[CrossRef](#)]
- Moayedi, H.; Aghel, B.; Abdullahi, M.M.; Nguyen, H.; Rashid, A.S.A. Applications of rice husk ash as green and sustainable biomass. *J. Clean. Prod.* **2019**, *237*, 117851. [[CrossRef](#)]
- Bhat, V.S.; Kanagavalli, P.; Sriram, G.; Prabhu, B.R.; John, N.S.; Veerapandian, M.; Kurkuri, M.; Hegde, G. Low cost, catalyst free, high performance supercapacitors based on porous nano carbon derived from agriculture waste. *J. Energy Storage* **2020**, *32*, 101829. [[CrossRef](#)]
- Li, Z.; Guo, D.; Liu, Y.; Wang, H.; Wang, L. Recent advances and challenges in biomass-derived porous carbon nanomaterials for supercapacitors. *Chem. Eng. J.* **2020**, *397*, 125418. [[CrossRef](#)]
- Zheng, S.; Zhang, J.; Deng, H.; Du, Y.; Shi, X. Chitin derived nitrogen-doped porous carbons with ultrahigh specific surface area and tailored hierarchical porosity for high performance supercapacitors. *J. Bioresour. Bioprod.* **2021**, *6*, 142–151. [[CrossRef](#)]

24. Yan, B.; Feng, L.; Zheng, J.; Zhang, Q.; Jiang, S.; Zhang, C.; Ding, Y.; Han, J.; Chen, W.; He, S. High performance supercapacitors based on wood-derived thick carbon electrodes synthesized via green activation process. *Inorg. Chem. Front.* **2022**, *9*, 6108–6123. [[CrossRef](#)]
25. Wei, L.; Deng, W.; Li, S.; Wu, Z.; Cai, J.; Luo, J. Sandwich-like chitosan porous carbon Spheres/MXene composite with high specific capacitance and rate performance for supercapacitors. *J. Bioresour. Bioprod.* **2022**, *7*, 63–72. [[CrossRef](#)]
26. Boundzanga, H.M.; Cagnon, B.; Roulet, M.; de Persis, S.; Vautrin-UI, C.; Bonnamy, S. Contributions of hemicellulose, cellulose, and lignin to the mass and the porous characteristics of activated carbons produced from biomass residues by phosphoric acid activation. *Biomass-Conv. Biorefinery* **2020**, *12*, 3081–3096. [[CrossRef](#)]
27. Cagnon, B.; Py, X.; Guillot, A.; Stoekli, F.; Chambat, G. Contributions of hemicellulose, cellulose and lignin to the mass and the porous properties of chars and steam activated carbons from various lignocellulosic precursors. *Bioresour. Technol.* **2009**, *100*, 292–298. [[CrossRef](#)]
28. Li, J.R.; Xu, J.R.; Zhang, M.Q.; Rong, M.Z. Carbon black/polystyrene composites as candidates for gas sensing materials. *Carbon* **2003**, *41*, 2353–2360. [[CrossRef](#)]
29. Hindermann-Bischoff, M.; Ehrburger-Dolle, F. Electrical conductivity of carbon black–polyethylene composites: Experimental evidence of the change of cluster connectivity in the PTC effect. *Carbon* **2001**, *39*, 375–382. [[CrossRef](#)]
30. Ayub, S.; Guan, B.; Ahmad, F.; Javed, M.; Mosavi, A.; Felde, I. Preparation Methods for Graphene Metal and Polymer Based Composites for EMI Shielding Materials: State of the Art Review of the Conventional and Machine Learning Methods. *Metals* **2021**, *11*, 1164. [[CrossRef](#)]
31. Lucian, M.; Volpe, M.; Gao, L.; Piro, G.; Goldfarb, J.L.; Fiori, L. Impact of hydrothermal carbonization conditions on the formation of hydrochars and secondary chars from the organic fraction of municipal solid waste. *Fuel* **2018**, *233*, 257–268. [[CrossRef](#)]
32. Watson, A.Y.; Valberg, P.A. Carbon Black and Soot: Two Different Substances. *AIHAJ-Am. Ind. Hyg. Assoc. J.* **2001**, *62*, 218–228. [[CrossRef](#)]
33. Gergova, K.; Petrov, N.; Eser, S. Adsorption properties and microstructure of activated carbons produced from agricultural by-products by steam pyrolysis. *Carbon* **1994**, *32*, 693–702. [[CrossRef](#)]
34. McDougall, G.J. The physical nature and manufacture of activated carbon. *J. S. Afr. Inst. Min. Metall.* **1991**, *91*, 109–120.
35. Daud, W.M.A.W.; Ali, W.S.W. Comparison on pore development of activated carbon produced from palm shell and coconut shell. *Bioresour. Technol.* **2004**, *93*, 63–69. [[CrossRef](#)]
36. Dong, M.; Li, Q.; Liu, H.; Liu, C.; Wujcik, E.K.; Shao, Q.; Ding, T.; Mai, X.; Shen, C.; Guo, Z. Thermoplastic polyurethane-carbon black nanocomposite coating: Fabrication and solid particle erosion resistance. *Polymer* **2018**, *158*, 381–390. [[CrossRef](#)]
37. Rampur, V.; Banagar, A.R.; Ganesh, U.L.; Srinivas, C.V.; Reur, S.C. Mechanical characterization of wood apple and coconut shell reinforced hybrid composites. *AIP Conf. Proc.* **2020**, *2247*, 040001.
38. González, J.; Román, S.; Encinar, J.; Martínez, G. Pyrolysis of various biomass residues and char utilization for the production of activated carbons. *J. Anal. Appl. Pyrolysis* **2009**, *85*, 134–141. [[CrossRef](#)]
39. Liyanage, C.D.; Pieris, M. A Physico-Chemical Analysis of Coconut Shell Powder. *Procedia Chem.* **2015**, *16*, 222–228. [[CrossRef](#)]
40. Sekhon, S.S.; Kaur, P.; Park, J.-S. From coconut shell biomass to oxygen reduction reaction catalyst: Tuning porosity and nitrogen doping. *Renew. Sustain. Energy Rev.* **2021**, *147*, 111173. [[CrossRef](#)]
41. Wang, L.L.; Zhang, L.; Tian, M. Mechanical and tribological properties of acrylonitrile–butadiene rubber filled with graphite and carbon black. *Mater. Des.* **2012**, *39*, 450–457. [[CrossRef](#)]
42. Jawhari, T.; Roid, A.; Casado, J. Raman spectroscopic characterization of some commercially available carbon black materials. *Carbon* **1995**, *33*, 1561–1565. [[CrossRef](#)]
43. Medalia, A.I. Electrical conduction in carbon black composites. *Rubber Chem. Technol.* **1986**, *59*, 432–454. [[CrossRef](#)]
44. Dannenberg, E.M. Bound rubber and carbon black reinforcement. *Rubber Chem. Technol.* **1986**, *59*, 512–524. [[CrossRef](#)]
45. Zbair, M.; Bottlinger, M.; Ainassaari, K.; Ojala, S.; Stein, O.; Keiski, R.L.; Bensitel, M.; Brahmi, R. Hydrothermal Carbonization of Argan Nut Shell: Functional Mesoporous Carbon with Excellent Performance in the Adsorption of Bisphenol A and Diuron. *Waste Biomass-Valorization* **2020**, *11*, 1565–1584. [[CrossRef](#)]
46. Huang, X.; Wu, S.; Du, X. Gated mesoporous carbon nanoparticles as drug delivery system for stimuli-responsive controlled release. *Carbon* **2016**, *101*, 135–142. [[CrossRef](#)]
47. Zhao, Q.; Lin, Y.; Han, N.; Li, X.; Geng, H.; Wang, X.; Cui, Y.; Wang, S. Mesoporous carbon nanomaterials in drug delivery and biomedical application. *Drug Deliv.* **2017**, *24*, 94–107. [[CrossRef](#)]
48. Azam, K.; Raza, R.; Shezad, N.; Shabir, M.; Yang, W.; Ahmad, N.; Shafiq, I.; Akhter, P.; Razzaq, A.; Hussain, M. Development of recoverable magnetic mesoporous carbon adsorbent for removal of methyl blue and methyl orange from wastewater. *J. Environ. Chem. Eng.* **2020**, *8*, 104220. [[CrossRef](#)]
49. Hong, Z.-Q.; Li, J.-X.; Zhang, F.; Zhou, L.-H. Synthesis of magnetically graphitic mesoporous carbon from hard templates and its application in the adsorption treatment of traditional Chinese medicine wastewater. *Acta Phys.-Chim. Sin.* **2013**, *29*, 590–596.
50. Azimi, E.B.; Badiie, A.; Ghasemi, J.B. Efficient removal of malachite green from wastewater by using boron-doped mesoporous carbon nitride. *Appl. Surf. Sci.* **2019**, *469*, 236–245. [[CrossRef](#)]
51. Ji, L.; Liu, F.; Xu, Z.; Zheng, S.; Zhu, D. Adsorption of Pharmaceutical Antibiotics on Template-Synthesized Ordered Micro- and Mesoporous Carbons. *Environ. Sci. Technol.* **2010**, *44*, 3116–3122. [[CrossRef](#)]

52. Wang, B.; Xu, X.; Tang, H.; Mao, Y.; Chen, H.; Ji, F. Highly efficient adsorption of three antibiotics from aqueous solutions using glucose-based mesoporous carbon. *Appl. Surf. Sci.* **2020**, *528*, 147048. [[CrossRef](#)]
53. Xin, W.; Song, Y. Mesoporous carbons: Recent advances in synthesis and typical applications. *RSC Adv.* **2015**, *5*, 83239–83285. [[CrossRef](#)]
54. Wang, Y.; He, C.; Brouzgou, A.; Liang, Y.; Fu, R.; Wu, D.; Tsiakaras, P.; Song, S. A facile soft-template synthesis of ordered mesoporous carbon/tungsten carbide composites with high surface area for methanol electrooxidation. *J. Power Sources* **2012**, *200*, 8–13. [[CrossRef](#)]
55. Panwar, N.L.; Pawar, A. Influence of activation conditions on the physicochemical properties of activated biochar: A review. *Biomass-Converts. Biorefinery* **2020**, *12*, 925–947. [[CrossRef](#)]
56. Li, W.; Yang, K.; Peng, J.; Zhang, L.; Guo, S.; Xia, H. Effects of carbonization temperatures on characteristics of porosity in coconut shell chars and activated carbons derived from carbonized coconut shell chars. *Ind. Crop. Prod.* **2008**, *28*, 190–198. [[CrossRef](#)]
57. Prauchner, M.J.; Rodríguez-Reinoso, F. Chemical versus physical activation of coconut shell: A comparative study. *Microporous Mesoporous Mater.* **2012**, *152*, 163–171. [[CrossRef](#)]
58. Marsh, H.; Reinoso, F.R. *Activated Carbon*; Elsevier: Amsterdam, The Netherlands, 2006.
59. Tu, R.; Sun, Y.; Wu, Y.; Fan, X.; Wang, J.; Shen, X.; He, Z.; Jiang, E.; Xu, X. Effect of surfactant on hydrothermal carbonization of coconut shell. *Bioresour. Technol.* **2019**, *284*, 214–221. [[CrossRef](#)]
60. Sajjadi, B.; Chen, W.-Y.; Egiebor, N.O. A comprehensive review on physical activation of biochar for energy and environmental applications. *Rev. Chem. Eng.* **2019**, *35*, 735–776. [[CrossRef](#)]
61. Downie, A.; Crosky, A.; Munroe, P. Physical Properties of Biochar. In *Biochar for Environmental Management*; Routledge: London, UK, 2012; pp. 45–64.
62. Bardestani, R.; Patience, G.S.; Kaliaguine, S. Experimental methods in chemical engineering: Specific surface area and pore size distribution measurements—BET, BJH, and DFT. *Can. J. Chem. Eng.* **2019**, *97*, 2781–2791. [[CrossRef](#)]
63. Wang, Y.; Zhang, Z.; Fan, H.; Wang, J. Wood carbonization as a protective treatment on resistance to wood destroying fungi. *Int. Biodeterior. Biodegrad.* **2018**, *129*, 42–49. [[CrossRef](#)]
64. Warren, B.E. X-ray diffraction study of carbon black. *J. Chem. Phys.* **1934**, *2*, 551–555. [[CrossRef](#)]
65. Heckman, F. Microstructure of carbon black. *Rubber Chem. Technol.* **1964**, *37*, 1245–1298. [[CrossRef](#)]
66. Ungár, T.; Gubicza, J.; Ribárik, G.; Pantea, C.; Zerda, T. Microstructure of carbon blacks determined by X-ray diffraction profile analysis. *Carbon* **2002**, *40*, 929–937. [[CrossRef](#)]
67. Kang, D.S.; Lee, S.M.; Lee, S.H.; Roh, J.S. X-ray diffraction analysis of the crystallinity of phenolic resin-derived carbon as a function of the heating rate during the carbonization process. *Carbon Lett.* **2018**, *27*, 108–111.
68. Donohue, M.D.; Aranovich, G.L. Classification of Gibbs adsorption isotherms. *Adv. Colloid Interface Sci.* **1998**, *76–77*, 137–152. [[CrossRef](#)]
69. Daud, W.M.A.W.; Ali, W.S.W.; Sulaiman, M.Z. The effects of carbonization temperature on pore development in palm-shell-based activated carbon. *Carbon* **2000**, *38*, 1925–1932. [[CrossRef](#)]
70. Rodríguez-Reinoso, F. Microporous structure of activated carbons as revealed adsorption methods. *Chem. Phys. Carbon* **1989**, *21*, 1.
71. Rodríguez-Reinoso, F. Controlled Gasification of Carbon and Pore Structure Development. In *Fundamental Issues in Control of Carbon Gasification Reactivity*; Springer: Berlin/Heidelberg, Germany, 1991; pp. 533–571.
72. Marquez-Linares, F.; Roque-Malherbe, R.M.A. Synthesis and Characterization of Large Specific Surface Area Nanostructured Amorphous Silica Materials. *J. Nanosci. Nanotechnol.* **2006**, *6*, 1114–1118. [[CrossRef](#)]

Disclaimer/Publisher’s Note: The statements, opinions and data contained in all publications are solely those of the individual author(s) and contributor(s) and not of MDPI and/or the editor(s). MDPI and/or the editor(s) disclaim responsibility for any injury to people or property resulting from any ideas, methods, instructions or products referred to in the content.